

Ultraluminous Infrared Galaxies and the Radio-Optical Correlation for Quasars

CAROL J. LONSDALE

*Infrared Processing and Analysis Center
California Institute of Technology, 100-22
Jet Propulsion Laboratory
Pasadena, CA 91125*

HARDING E. SMITH¹

*Center for Astrophysics and Space Sciences
and
Department of Physics,
University of California, San Diego
La Jolla, CA 92093 0111*

COLIN J. LONSDALE

*Haystack Observatory,
Massachusetts Institute of Technology
Off Route 40
Westford, MA 01886*

Subject headings: galaxies: quasars infrared: galaxies radio continuum: galaxies

¹also, Infrared Processing and Analysis Center, Jet Propulsion Laboratory, California Institute of Technology

ABSTRACT

Through analysis of available optical spectrophotometric data and radio flux density measurements in the literature, it is demonstrated that a good correlation exists between the radio power and bolometric luminosity of the optically-selected QSOs in the Bright Quasar Sample (BQS) of Schmidt and Green (1983). This correlation, noted previously by others as a correlation with absolute B magnitude, is shown to be robust, and to be independent of a variety of assumptions used in the calculation of the bolometric luminosity. The correlation is present for the entire BQS sample, but is improved when QSOs with high values of radio-to optical flux density (radio-loud) are excluded. Using this correlation, radio measurements can therefore be used to predict the bolometric luminosity of quasars even if their optical and UV continua are not directly observable.

We have recently used VLBI measurements of a sample of ultraluminous infrared galaxies to infer the likely existence of radio-quiet AGN deeply enshrouded in dust within their nuclei (Lonsdale, Smith and Lonsdale 1993). We employ the radio-bolometric luminosity correlation for the BQS quasars to test whether these hypothetical buried AGN can be energetically responsible for the observed far-infrared luminosities of the ultraluminous infrared galaxies. The ultraluminous infrared galaxies are shown to follow the same relation between radio core power and bolometric luminosity as the radio-quiet QSOs, suggesting that buried AGNs can account for essentially all the observed infrared luminosity, and raising the possibility that any starburst which may be in progress may not be energetically dominant.

The broader implications of the radio-optical correlation in quasars for AGN and luminous infrared galaxy (LIRG) use of radio astronomy as a probe of the central powerhouse in radio-quiet AGNs and luminous infrared galaxies are briefly discussed.

1. INTRODUCTION

It has been recognized for some time (Miller, Peacock and Meade 1990, Stoake *et al.* 1992) that the quasar population can be divided into two separate groups, so-called *radio-loud* and *radio-quiet* quasars, primarily based on the ratio, R , of radio to optical flux density. As complete quasar samples have been extended to greater distances and numbers, more sensitive tests of the apparent bimodality of the R distributions have become possible, and the existence of two separate physical classes of quasar based on radio loudness no longer seems to be in question (Stoake *et al.* 1992, hereafter SMWF). Further, SMWF noted that a strong correlation exists between radio and optical luminosities for the radio quiet objects in the BQS, the only sample which as yet enjoys a high rate of radio detections (Kellermann *et al.* 1989). According to SMWF, the probability of a chance correlation of the observed strength is less than 0.1%, but this estimate is obtained without a complete treatment of the radio non-detections in the sample, and does not explicitly address possible selection effects in this optical flux density limited sample. Also, the application of a radio-quietness criterion, which represents a boundary of unity slope in the radio/optical luminosity plane, complicates assessments of correlation significance.

In this paper, we confirm the reality of this correlation for the BQS quasars by independently deriving a measure of optical/UV luminosity from the spectrophotometric data of Neugebauer *et al.* (1987), using survival analysis techniques to treat the presence of upper limits in the radio data and considering sample selection effects. We find that the correlation is strong, and does not depend on the method of luminosity calculation employed. By performing interpolations between the observed optical/UV and soft X-rays using two different methods, we demonstrate that the radio power is correlated not only with optical luminosity, but with the estimated luminosity of the big blue bump (BBB) which dominates the bolometric luminosity of these objects (ignoring hard X-rays and γ -rays, in which the BQS is not well observed).

The search for such a correlation, particularly involving the bolometric luminosity of the quasars, was motivated by a desire to test the hypothesis that the ultraluminous infrared galaxies (ULIRGs) are powered by dust-enshrouded AGNs. In a previ-

ous study (Lonsdale, Smith and Lonsdale 1993; hereafter LSL), we showed that a large fraction of the ULIRGs with $L_{IR} > 10^{11.25} L_{\odot}$ contain high brightness temperature radio sources in their nuclei, which typically account for of order 10% of the total radio flux density at 18cm wavelength. The median VLBI core power for the detected sources is $10^{22} \text{ W Hz}^{-1}$, which is comparable to the power of many radio quiet QSOs (RQQ), and much greater than the compact radio sources seen in quiescent late-type galaxies. In another recent result we have found strong evidence that the OH megamaser emission in the prototypical ultraluminous infrared galaxy, Arp 220, is dominated by parsec-scale emission (Lonsdale *et al.* 1994). This emission probably arises in a molecular torus surrounding an AGN, and may require a large fraction of the observed far-infrared power to pump the maser, thus this result supports the picture in which most of the far-infrared emission of Arp 220 originates in an AGN and not a circumnuclear starburst. If Arp 220 is representative and if the VLBI-scale continuum sources represent emission from normal radio-quiet quasars embedded in the dusty nuclei, we can use the above-mentioned relationship between RQQ radio power and bolometric luminosity to estimate the quasar power available for dust reprocessing into the far-infrared, and compare that quantity to the observed infrared luminosity.

We are able to demonstrate that buried RQQs of bolometric luminosities implied by our VLBI-scale flux densities are indeed capable of powering the entire infrared luminosity of the ULIRGs (though the calculations are necessarily uncertain to roughly a factor of two, and admit the possibility of comparable contributions to the far-infrared luminosity from an AGN and a starburst).

In section 2 we describe the data used to establish the quasar correlation, and in section 3 we give an account of the statistical methods used, together with a brief discussion of possible selection and other effects in the dataset. Section 4 deals with the application of the correlation to the ULIRG sample observed by us with VLBI, and in section 5 we discuss the broader implications of both results, including the likelihood that both AGNs and starbursts contribute significantly to the luminosity of ULIRGs, and further observational tests to answer this question.

2. THE BQSRADIO AND BOLOMETRIC (IR X-RAY) DATA

2.1. The Radio Data

Kellermann *et al.* (1989) have observed all 114 BQS quasars at 5 GHz. Their typical detection threshold is approximately 0.2 mJy, depending on the degree of positional coincidence with the optical QSO, and the somewhat variable integration time per source. They list measured flux densities on two different angular scales, referring to the values from their low (~ 18 arcsec) resolution data as the total flux density, and those from their high ($\sim 0''.5$) resolution observations as the core flux density. Because the original motivation behind the present work was to allow a comparison between the radio powers of RQQs with those from the VLBI detections of 111,117s, we used the core flux densities whenever possible. The core flux densities are also likely to be contaminated by chance superpositions with unassociated foreground or background radio sources. However for completeness, and to assess the effects of different amounts of upper limit data in the analysis, we performed a similar correlation analysis using the total flux densities. In cases where the $0''.5$ resolution observations were unavailable, we instead used the total flux density, or limit thereon, as an upper limit to the core flux density. SMWF note that for one source, 1211-114, the flux density quoted by Kellermann *et al.* is in error due to misidentification with a fainter background quasar. We adopt the corrected value of 0.8 mJy obtained by SMWF via a private communication from Kellermann (1991) as an upper limit to the core flux density.

The resulting core flux density dataset comprised roughly 60% detected values, and 40% upper limits. Because of the above manner in which these limits were assigned, they tend to be well-mixed with the detected values and in principle the valuable information they contain is recovered through the use of the techniques for survival analysis (see Section 3). Although other optically-selected quasar samples have been surveyed using sensitive radio telescopes (most notably a subset of the LBQS, Visnovsky *et al.* 1992), the fraction of censored data for the radio quiet objects in these samples is too high to allow meaningful investigation of any relationship between their radio and optical luminosities.

2.2. Optical to Ultraviolet Integrations

Both previous studies in which the optical/radio correlation was noted (Miller, Peacock and Meade 1990 and SMWF) used K-corrected optical luminosities derived from the B magnitude. However, an extensive database of optical, UV and X-ray information is available in the literature, in the form of detailed optical spectrophotometry for most of the BQS by Neugebauer *et al.* (1987), IUE measures by Sun and Malkan (1989) and X-ray observations by Tannenbaum *et al.* (1986). The overall continuous energy distributions of the BQS sample are excellently summarized in Sanders *et al.* (1989). The intersection of the Neugebauer *et al.* list of quasars and the Kellermann *et al.* list comprises 97 objects. We have used these data to calculate integrated luminosities over well-defined rest-wavelength intervals as estimates of the bolometric QSO luminosity for this sample. This method obviates the need to perform error-prone K-corrections, which inaccurately assume the same spectral shape for all objects in the sample.

In addition to the spectrophotometry of Neugebauer *et al.* we have included IUE observations for 29 QSOs from Sun and Malkan (1989). For 3 additional objects with IUE observations we found that the IUE spectra did not match the high frequency end of the Neugebauer *et al.* spectrophotometry well in flux level, so these IUE spectra were not used in our integrations. We believe that these discrepancies are due to a combination of IUE pointing errors, aperture size differences and flux variability (Malkan 1993, private communication).

We performed integrations over the optical to ultraviolet wavelength range in a two different ways in order to test the sensitivity of the results to the integration method. The most conservative method is to integrate only over that portion of the rest frequency range for which data is available for all QSOs in the sample: $14.6 < \log \nu_{rest} < 15.0$. We refer to this as the optical or "O" integration and the integrated luminosity as " L_O ", (3000 Å to 7500 Å); it utilizes the Neugebauer *et al.* spectrophotometry only, *i.e.* the IUE data are not included.

In a second method, which we refer to as O-UV, we include the IUE data, where available, to extend the coverage to higher frequencies imposing uniform upper and lower frequency limits, $14.5 < \log \nu_{rest} < 15.3$. This spectral range is covered by reliable measurements for a reasonable fraction of the sample.

Interpolation between measured IUE data points or extrapolation from the highest frequency IUE data point is then performed for each quasar spectrum to obtain coverage over this rest frequency range. When extrapolation was necessary, it was accomplished by a least squares power-law fit to the 10 highest frequency data points of the spectrum.

2.3. Extension to X-ray Energies

Most of the luminosity in quasars arises in the so-called big blue bump (BBB), which manifests itself observationally as a rising spectrum in the blue and near-UV, and a sharply negative soft X-ray spectral index (defined in the sense $S_\nu \propto \nu^\alpha$) in many cases (Wilkes and Elvis 1987, Canizares and White 1989). Unfortunately the bulk of the luminosity of the BBB lies in the unobservable far-UV. Estimation of the integrated optical-to-X-ray luminosity of a quasar therefore requires interpolation between measurements at optical/UV wavelengths and soft X-rays to estimate the far-UV.

Among the models for the BBB are thermal accretion disk models (Sun and Malkan 1989), synchrotron models (Burbidge, Jones and O'Dell 1974) optically thin free-free models (Barvainis 1993) and combinations of these (Puetter *et al.* 1982). The predicted spectral shape of the BBB differs somewhat between these models. Rather than attempting to fit the BQS data with detailed fits to these models, we used a combination of available observational constraints on the BBB shape and the broad similarities between the theoretically predicted shapes to arrive at two simple and reasonably representative methods of estimating the integrated BBB luminosity, following Saunders *et al.* (1989). The UV data of O'Brien, Gondhalekar and Wilson (1988) indicate that the UV continuum spectral indices between $\log \nu = 15.2$ and 15.4 are a function of luminosity, ranging from -0.4 to -1.0 for their sample, and these spectral slopes are steeper than those of the optical/UV continuum, which appears to have a median value of -0.2 in the BQS (Neugebauer *et al.* 1987). Steepening of the observed continuum slopes due to starlight contamination in the lower luminosity objects may be present (*c.g.* Barvainis 1990), but for our purposes the effects are likely to be negligible, and we will ignore this potential effect.

We determined the flux density of each quasar at the highest rest frequency, reliable IUE observation, ν_{UV} . In the absence of IUE data, $\log \nu_{UV} = 15.3$ was

adopted. If a measured flux density at $\log \nu_{rest} = 15.3$ was not available, the flux density was extrapolated by least-squares fitting of a power-law to the 10 highest frequency data points from Neugebauer *et al.* (1987).

We then used two interpolation methods to calculate integrated optical X-ray luminosities using the *Hubble Space Telescope* observations of the BQS published by Tannenbaum *et al.* (1986). The first, which we designate *O-X1*, employs a simple power-law fit from $\log \nu_{rest} = \log \nu_{UV}$ to the rest frequency of the measured 2 keV point at $\log \nu_{obs} = 17.68$. 60 of the QSOs in our sample of 97 have *Hubble Space Telescope* observations; in the remaining 37 cases for which no X-ray measurements are available, we used the median *Hubble Space Telescope* slope from the sources with X-ray data for extrapolation. We regard *O-X1* as a conservative lower limit to the contribution to the total luminosity from the unobservable BBB. The second method, *O-X2*, which may yield a more realistic estimate of the BBB luminosity, employs an assumed $S_\nu \propto \nu^{-1}$ spectral shape between $\log \nu_{rest} = \log \nu_{UV}$ and $\log \nu_{rest} = 16.5$ (i.e. flat in νf_ν), followed by a power-law extension from $\log \nu = 16.5$ to $\log \nu = 17.78$. Again, for objects with no measured X-ray flux, we used the median interpolated slope from the objects with X-ray data. It was judged that the reliability and consistency of the available data, particularly between the observed optical spectrophotometry and IUE measures which most significantly affect BBB fits, did not justify more elaborate interpolation schemes. The two interpolation methods are illustrated in Figure 1.

The effects of these two interpolation methods are to place different degrees of emphasis on the shortest-wavelength measurements of Neugebauer *et al.* (1987) and/or the IUE data. L_{O-X1} is weighted more by the integrated optical luminosity, while the L_{O-X2} is weighted more by the blue end of the observed range. Of the two interpolations, L_{O-X2} more closely reflects current knowledge of the UV continuum slopes. In the luminosity range of primary interest for this work ($\sim 10^{45} \text{ erg s}^{-1}$), the far-UV slope, $\alpha_{uv} = -1$, assumed in the *O-X2* interpolation is plausible, given the results of O'Brien, Gondhalekar and Wilson (1988). The *O-X2* interpolation also agrees well with the predictions of the free-free model for the BBB, with a relatively low temperature, $T \sim 10^5 \text{ K}$, appropriate to AGNs with such luminosities (Barvainis 1993). The *O-X1* interpolation more closely reflects the predicted spectral shapes from accretion

disk models (Sun and Malkan 1989). It is important to recognize that these interpolations provide, at best, poor approximations to the (true) BBB luminosity since it is only the long-wavelength tail which is accessible to us. However, because we feel that the integrated luminosity including the dominant BBB is a more fundamental parameter than the optical luminosity, we expect that our integrated luminosities will permit more sensitive statistical searches for physically meaningful relationships. More accurate BBB luminosity determinations must await improved space-based UV observations.

2.4. Infrared Data

Finally, we included the available mid to far-infrared IRAS data for the sample of 51 objects with IRAS detections from Sanders *et al.* (1989) in an integrated luminosity designated $IR-X2$. The available IRAS data were included in the integration using the lowest frequency ($\nu_{rest} = \nu_{IR}$) IRAS data point as the lower limit of integration. This integration suffers from non-uniform integration limits. Furthermore, the correct treatment of the RQ/IR emission is geometry dependent. In the case of non-spherically symmetric dust distributions in the RQs (*e.g.* a warm, dusty nuclear torus), inclusion or omission of the IR emission can lead to either an under- or overestimate of the true bolometric luminosity, because the presence of an asymmetric dust distribution implies an anisotropic escape of optical/UV radiation. The ratio of the mean integrated infrared X-ray luminosity to the mean optical X-ray luminosity, $\log(\langle L_{IR-X2} \rangle / \langle L_{O-X2} \rangle) = 0.24$. Given the difficulty in interpretation and the relatively small contribution of the infrared, we have ignored it in the analyses that follow.

Table 1 summarizes the five different integrated luminosities, along with the monochromatic radio power at 6cm emitted wavelength. Column (1) lists the QSO coordinate name, column (2) gives the redshift, columns (3) & (4), give the start and end rest frequencies, of the Neugebauer *et al.* spectrophotometric measurements, columns (5) and (6) give the optical and optical-ultraviolet integrated luminosities calculated as described in the text above, column (7) gives ν_{UV} , the highest rest-frequency UV point, columns (8) & (9) give the optical X-ray luminosities, calculated as described in §2.3, column (10) gives the infrared X-ray luminosity for those BQS QSOs with IRAS detections, column (11) gives the lowest rest

frequency IRAS detection, ν_{IR} , and columns (12) and (13) give the total and core radio power, respectively, from Kellermann *et al.* All quantities are computed for a standard Friedmann cosmological model with $H_0 = 75 \text{ (} \pm 7 \text{)} \text{ s}^{-1} \text{ Mpc}^{-1}$ and $q_0 = 0$. We performed statistical tests using these various integrated luminosities, as summarized in Table 2.

3. STATISTICAL ANALYSIS OF THE BQS SAMPLE

The presence of radio upper limits in this sample dictates the use of the techniques of Survival Analysis (*e.g.* Isobe, Feigelson and Nelson 1986, and references therein). This dataset is well-matched to such techniques which perform best when censoring (limits) in the data are randomly distributed, because the radio flux-density limits correspond to a wide range of radio powers, which are well mixed with values for detected objects. For this reason we primarily investigate the presence of the correlation between radio and integrated optical data in the luminosity-luminosity plane rather than the flux-flux plane. Since there is a very high completeness of optical observations of this radio-selected sample (97/114 = 85%), there is little concern that use of the luminosity-luminosity plane will introduce a spurious distance-related correlation; however to verify this we have checked the reality of the results by also performing the statistical tests in the flux-flux plane. The luminosity-luminosity correlation statistics are presented here, but the flux-flux results are in all cases comparable.

We first examine the relationship between radio power and integrated luminosity for the BQS. A number of studies have examined this relationship for the BQS (Miller, Peacock and Meade 1990; SMWF), particularly with a view toward determining whether there is a true bimodality between radio-quiet and radio-loud QSO populations. Figure 2a shows the relationship between *total 6cm radio power*, P_{total} , within the 18" VLA beam of Kellermann *et al.* and *integrated optical luminosity*, L_O , for the BQS sample as described above. This relation is most directly comparable to the previous studies. Figures 2b, 2c and 2d show the same relationship using the *integrated optical UV luminosity*, $L_{O,UV}$, and the two methods of calculating the *integrated optical X-ray luminosity*, L_{O-X1} and L_{O-X2} , respectively. The relationships are quite similar; L_{O-X1} is on average about 0.4 dex higher than $L_{O,UV}$ and L_{O-X2} is on average

about 0.2 dex higher yet.

Figure 3 shows the relationship between *6cm radio core power*, P_{Core} , and integrated luminosity as in Figure 2; in this case we have employed the total 6cm power as an *upper limit* for those objects without high resolution radio observations. In each diagram there are 97 QSOs plotted with 16 and 40 upper limits on the total and core power, respectively. The apparent correlation between radio power and optical luminosity seen by other investigators is evident, as is the apparent radio loud/radio quiet separation in the diagram. Because the definition of “radio-loudness” is as yet imprecise, and different samples appear to show different sensitivities depending upon whether a definition is made in terms of radio power (Miller, Peacock and Meade 1990) or radio-to-optical flux density ratio (SMWF), we have opted to consider the significance of a putative radio-optical correlation on the entire sample without imposing such distinction.

The distributions in Figures 2 and 3 may be seen to be comparable; in §4 we will be principally concerned with the relationship between *radio core power* and *integrated luminosity*; therefore we will discuss in detail the statistical test results for Figure 3d - P_{Core} vs L_O . χ^2 , which we believe may be the best estimator of bolometric luminosity - but the results for Figures 2 and 3 are in all cases comparable, with a somewhat higher level of significance for the relations in terms of P_{Total} (Figure 2) due to the fewer upper limits in the distribution.

We have employed two correlation tests from the *ASURV* Software Package (provided to *IPAC* by E. Feigelson and T. Isobe) for Survival Analysis of censored data: Cox’s Hazard Test (parametric, assuming a Gaussian error distribution) and the Generalized Kendall’s Tau (BHK, nonparametric) Test, with equivalent results. For the data in Figure 3d, for example, the Cox-Hazard Test finds a positive correlation with a $\chi^2 = 37.25$ for 1 degree of freedom, and both tests find the likelihood that the parameters are uncorrelated to be less than 10^{-4} . This result is quite robust, with comparable or better significance level for all definitions of integrated luminosity and for both core and total radio power. Similarly, we have repeated the tests for a variety of Friedmann cosmologies ($h_0 = 0.5 - 1.0$; $\Omega_0 = 0 - 1$; $\Lambda = 0$) with negligible effect on the level of statistical significance. We note that this correlation also exists in the relationship between radio and optical flux-density; in this case, however, the application of the above statistical methods

is questionable because the censoring, applied in the form of a near-uniform 0.25 mJy sensitivity limit, is **1101** random in radio flux-density. Although there is relatively little difference in the significance of the result among the estimators of luminosity, the smallest dispersion is for L_O , the optical luminosity, which is fully measured for all objects in the sample. We believe that it is likely that we artificially inject dispersion into the sample by the assumptions in our interpolation/extrapolation methods. The difference in significance between the P_{Total} and P_{Core} relations is entirely explained by the relatively larger number of limits to the radio core power.

We have also employed linear regression analysis (parametric EM Method, also from the *ASURV* Package) to fit power-law relations of the form, $\log P(6cm) = a \cdot \log L + b$.

Table 2 gives the complete set of statistical results for the Radio Power - Integrated Luminosity Correlations for the three sets of tests: Cox-Hazard, BHK, and EM Method. (D11111111) lists the calculated integrated luminosity estimators, separated into the three samples (BQS, BQS*, and BQS*+ULIRG) as described in the text below. Along the line giving the sample identification are numbers denoting the sample size/number of limits in the sample. Columns (2) and (3) give the value of χ^2 calculated by the Cox-Hazard correlation test for Total 6cm Radio Power and Core Radio Power, respectively. Columns (4) & (5), similarly, give the values of Kendall’s τ as calculated by the BHK Correlation (4(5), Columns (6), (7), and (8), give the values of the slope, “a” ($\pm \sigma_a$), the intercept, “b” ($\pm \sigma_b$), and standard deviation of the regression, σ_{fit} for the Total Radio Power vs. Integrated Luminosity relations, respectively, and columns (9) (11) give the same data for the Core Power vs. Integrated Luminosity Relations. Statistical results for the combined BQS*+ULIRG sample are given only for the Core Power analysis, since that is the only potentially meaningful physical relationship. In all cases except one the probability, estimated by the Cox-Hazard and BHK tests, is less than **10⁻⁴** that the data could come from uncorrelated quantities. The lone exception is the P_{Core} vs. L_O relation for the combined sample, for which the probability is about 3% as calculated by Cox-Hazard, and 0.1% as estimated by BHK that the data are uncorrelated.

We must, of course, be concerned with selection effects in the BQS sample. For example, SMWF discuss the possibility that the BQS may be incor-

plete in the redshift interval, $0.6 \leq z \leq 1.0$, due to “red-denning” of the QSO $U - B$ color by the presence of Mg II and Fe II emission features in the B-band over that redshift range. In Figure 4, we show the 6 cm Radio Core Power as a function of integrated optical X-ray luminosity, $L_{0.3-2}$, for the BQS sample, restricted to QSOs with redshift, $z < 0.6$, and, in this case, to radio-quiet objects (radio-optical flux-density ratio, $\log R < 1$, from Kellermann *et al.*). This sample, which we designate “BQS”, was constructed as a match to the Ultraluminous IR Galaxy sample described in §4 and also to eliminate the possible selection imposed by the above effect. Visual inspection suggests a tighter relationship, in particular due to the exclusion of radio-loud QSOs, but the relatively larger fraction of radio limits decreases the significance of the result. In this case there are 61 objects with 29 limits and $\chi^2 = 22.1$ (Cox’s Hazard Test), with both tests estimating a likelihood less than 10^{-4} that the parameters are unrelated. The solid line in Figure 4 is the linear regression fit by LM Method given in Table 2. (Regression analysis by non-parametric, Buckley-James regression method is indistinguishable.)

4. EMBEDDED QUASARS IN ULTRALUMINOUS IR GALAXIES

LSI performed an 18 cm VLBI survey of 31 ULIRGs, taken from the high resolution 8.44 Survey GHz by Condon *et al.* (1991, CHYT1) of the 40 most luminous members ($L_{IR} > 10^{11.2} L_{\odot}$) of the Bright Galaxy Sample (BGS) of Soifer *et al.* (1989). The BGS is a 60 μ m-limited sample ($S_{60\mu m} > 5.4 Jy$). Our selection criterion for the 31 galaxies observed with VLBI was that the object should have sufficient flux on the scale of the 0.725 VLBA beam to be potentially detectable by the most sensitive VLBI systems. LSI found that 17 of the 31 galaxies surveyed with VLBI showed high-brightness temperature emission, with $T_b > 10^5$ K and structure on scales of 5-150 mas. The VLBI observations thus cover over 75% of the complete 60 μ m flux and FIR luminosity-limited sample of Condon *et al.*, resulting in 43% 18 cm detections and 35% limits to the 18 cm core flux density and luminosity. The 9 sources eliminated from the CHYT1 sample are well mixed in L_{IR} and simply fail to meet our VLBI flux density observability criterion due to large distance; there is no apparent reason to suspect that the selection might strongly influence the correlations described below.

In a similar way to the BQS quasars, we have compared the radio power of the ULIRGs to their estimated bolometric luminosity. The radio power at 6 cm is estimated from the measured 18 cm power in order to allow a direct comparison to the observations of the BQS by Kellermann *et al.* (1989). The 18 cm powers were derived from the maximum correlated flux densities on baselines of projected length $\geq 10^5 \lambda$ (see LSI, for details); 17 of the 31 ULIRGs were detected by this criterion. The correction to 6 cm was done assuming a power law spectrum and the 1.49-8.44 GHz spectral index, $\alpha_{1.49}^{8.44}$, derived by CHYT1 and listed by LSI. Since these spectral indices were measured on significantly larger spatial scales than the VLBI emission, they may not be appropriate for our purposes, therefore as an alternative we also derived the corrections assuming a fixed spectral index, $\alpha = 0.5$ ($f_{\nu} \propto \nu^{-0.5}$) for all sources, following Kellermann *et al.* (1989). On the other hand, if free-free optical depths are large at 6cm, as suggested by CHYT1 and confirmed by LSI, then the observed $\alpha_{8.44}^{8.44}$ will provide a better estimate of the true 6cm core flux density. The effect of these different choices for the spectral index was found to be negligible. We note that the the χ^2 dependence of the free-free absorption cross-section implies that the high frequency radio continuum is unobscured, even if there is significant absorption near .5GHz.

The bolometric luminosity of the ULIRGs was simply taken to be the infrared luminosity, as derived by Soifer *et al.* (1989). This luminosity includes a bolometric correction for emission over the entire infrared (1-1000 μ m) region and assumes isotropic emission. Unlike the BQOs, the ULIRGs emit the vast majority (typically over 90%) of their total power in the far-infrared wavelength region. There is strong evidence for dense concentrations of molecular gas within the central few hundred parsecs of these objects, with extremely large optical depths such that essentially all the UV and optical energy generated within this region is effectively absorbed and re-radiated at far-infrared wavelengths (*cf.* Scoville 1992).

We have plotted in Figure 5 the VLBI core power as a function of FIR luminosity for the Ultraluminous Infrared Galaxies. For direct comparison, we also replot in this figure the redshift-limited $O-X^2$ integrated luminosity vs. P_{core} data for the BQS from Figure 4. As described in Smith, Lonsdale and Lonsdale (1994), there is not a statistically significant correlation between the VLBI core power and FIR lu-

minosity for the ULIRGs alone ($\chi^2 = 3.71$), but the ULIRGs clearly fall along a similar relationship to the low redshift, radio-quiet BQS QSOs. Although we are not aware of survival tests for the similarity of these two distributions we have used the above correlation/regression tests on the combined BQS/ULIRG data set (92 objects; 32 limits) to test the similarity of the relationship. In this case, inclusion of the 111,111 sample improves the significance of the result: $\chi^2 = 22.0$ vs. 25.7 when compared with the pure BQS sample. A regression fit to the combined data set is virtually indistinguishable from the fit to the BQS sample shown in Figure 4. The result, using $L_{0.1}$ is virtually identical; the results for other estimators of integrated luminosity have somewhat poorer significance, because the ULIRG and BQS distributions follow relations displaced in luminosity, that is, we need the true, optical X-ray luminosity of the putative AGN to power a luminous FIR Galaxy at comparable radio core power.

5. DISCUSSION

A crucial aspect of this result is the utility of radio measurements as a tracer of the power output of the central engine. Despite the fact that the integrated radio luminosity of the average MCG, from, say, 10 MHz to 10 GHz is 10^6 times lower than the bolometric luminosity of the quasar, this ratio is remarkably constant across the RQQ population. We have illustrated this utility in the case of hypothetical RQQs buried inside ultraluminous IR galaxies, but there is a more general class of applications for this result. The total power output of AGNs is frequently subject to great uncertainty, due to unknown obscuration and unknown anisotropy of the emission due to relativistic beaming and/or non-spherical obscuration. Potentially, the intensity of the cm-wavelength radio emission in the radio quiet AGN case may avoid these pitfalls, and serve as a unique diagnostic of these obscuration and anisotropic effects. Optical depths to cm-wavelength radiation are usually negligible in circumnuclear galactic environments, even for the extremely compact ULIRGs. If radio bolometric luminosity relation holds across the radio-quiet segment of the extragalactic zoo of active nuclei, and if the RQQ radio emission is isotropic (which we as yet have no reason to doubt), sensitive radio flux density measurements may become the tool of choice to establish arguably the most important parameter of an AGN, its luminosity. In cases where dust and gas are preva-

lent (e.g. Sy2 obscuring tori), radio observations may be our only probe of the nucleus.

The fact of this correlation is surprising, given the evidently disparate mechanisms for the production of radio and optical/UV emission in radio quiet quasars. The recent demonstration by Lonsdale and Barvainis (1994) that the radio emission in radio-quiet AGNs frequently displays high (non-thermal) brightness temperatures strongly suggests that the emission is due to synchrotron radiation, as in radio loud objects. By contrast, most of the bolometric luminosity in RQQs appears to be thermal in nature, even though there is heated debate regarding the location of the thermally emitting material. It is far from clear why radiation emitted by completely different mechanisms, and possibly from quite different regions of the AGN, should be so closely related.

The bimodality of the distribution of radio to optical flux density ratios described above is an important clue to this puzzle. The distribution of R , the radio to optical ratio, for the radio loud population is extremely broad, covering several orders of magnitude. This distribution is statistically dramatically different from the well-defined peak shown by the RQ quasars. Either the two component luminosities have a sharply truncated distribution near the RL/RQ boundary at $\log R = 1.0$, as suggested by SMWF, or this broad distribution extends well into the range of the radio quiet quasars. The evidence from the BQS is that few if any quasars lie below $\log R \sim 1$ (Kellermann *et al.* 1989). This strongly suggests that a two component model for quasar radio emission is appropriate. The first, and better known component would be the one responsible for the radio emission from radio loud quasars, identified with a parsec-scale relativistic jet laced with synchrotron plasma. We will refer to this as the RL component. The second component, which we dub the RQ component, may be present in all quasars, but would be swamped by the more powerful RL component in radio loud objects. Only when the RL component was extremely weak or absent would the flux density of this hypothetical RQ component be measurable. It is the luminosity of the RQ radio component which correlates well with the bolometric luminosity of the quasar in this picture. Alternately, a switch mechanism must operate which selects between the RL (e.g. relativistic jet) mechanism at high R and RQ (i.e. non-relativistic wind) emission at $\log R \approx 0$. We confine our discussion here to the RQ component.

Unfortunately, we have very limited observational information with which to infer the properties of this RQ component. The results of Lonsdale and Barvainis (1994) suggest, but do not prove, that the component has a scale size of less than a few parsecs. Spectral information on the component is almost nonexistent, the most extensive work to date being that of Antonucci and Barvainis (1988) who demonstrated that spectral indices exhibit a wide range in a small heterogeneous sample of RQQs. They (1KW) attention to the occasional presence of flat spectra at high frequencies, speculating that such emission may be thermal in origin. To our knowledge, no polarization information is available. Because of sensitivity considerations, it is difficult to observe objects which, in the above two component picture, we are confident are dominated by the RQ component. Consequently, even the above tentative inferences are subject to the possibility of substantial contamination from a weak RL component. Until new data are available, we are reduced to speculation on the possible nature of this RQ component, knowing only that it may be compact, and that its power is highly correlated with the bolometric luminosity of the quasar.

One possibility is that the RQ component is indeed compact, and that it is due to synchrotron radiation. In many astrophysical contexts, synchrotron radio emission occurs as a result of electron acceleration in shocks, and we can speculate that the mechanical energy necessary to drive the accelerating shocks originates from the radiation pressure of the central source, thus producing the observed correlation with bolometric luminosity. Another possibility, mentioned by Antonucci and Barvainis (1988) is that the emission is not compact, and represents the low-frequency tail of a centrally-heated thermal component. For this to be the case, the VLBI detections of Lonsdale and Barvainis (1994) would have to be due to a contaminating RL component. Detailed spectral and polarization information on a sample of RQQs is required to address these various possibilities, and will be reported elsewhere.

We have used this correlation to investigate the hypothesis that the ULIRGs in our sample contain embedded AGNs. If the VLBI-scale radio emission from ULIRGs originates in normal radio quiet AGNs, the implied bolometric luminosity, reprocessed by circumnuclear dust into the IR, is roughly equal to the observed FIR luminosity with an uncertainty of order a factor of two. This result lends considerable support

to the notion that the most compact, highest luminosity IR galaxies are powered in large part by a buried AGN, and provides room for doubt that a major part of the luminosity is supplied by a starburst. Any model which invokes a nuclear starburst as the energetically dominant component must include the postulate that the VLBI-scale emission comes from something other than a normal RQQ, specifically something with a ratio of radio to bolometric luminosity significantly higher than that of RQQs. Candidates might include clusters of ultraluminous radio supernovae (but see LSL for observational evidence severely constraining such a model), and anomalously radio loud AGNs, their properties presumably modified by the dense medium in which they must be embedded.

An important question to resolve concerns the origin of the intermediate-scale radio emission from the ULIRGs. Only $\sim 10\%$ of the total 1.6 GHz radio emission was typically detected in our VLBI experiment. The remaining $\sim 90\%$ originates on larger size scales, 0.05 to 0.5 arcseconds, or typically a few hundred parsecs, and has a characteristic brightness temperature of 10^3 to 10^5 K (see LSL, (11)). We cannot reasonably attribute this emission to normal RQQs, because the implied bolometric luminosities would be excessive, moving the ULIRGs well off the relationship for the RQQs in Figure 4. Fundamentally, the question is "Why does the core radio emission follow the RQQ radio/optical relation described above, while the intermediate scale emission (corrected by (1) for putative free-free extinction, see below) roughly follows the radio-infrared relation for 'normal' infrared-bright galaxies?"

(1) attribute this few 100 parsec scale emission to compact starbursts, and explain the flatness of the radio spectra of many objects by free-free absorption in the dense interstellar medium which has been inferred to exist on these size scales from interferometric molecular line studies (eg. Scoville 1992) in the ULIRGs. They also explain the significant departures of several objects from the well established, excellent correlation between global FIR and radio flux for galaxies (Helou, Soifer and Rowan-Robinson 1986), by such absorption. This is an appealing explanation for the few 100 parsec scale radio emission, and, if it is correct, we deduce that the contribution of the starburst to the total FIR luminosity for the objects in our sample is roughly comparable to the contribution from the hypothetical buried AGN.

In this picture the question arises as to why the

starburst and AGN luminosities should be comparable in our sample, and why we do not have many objects in which either the starburst or the AGN dominates? We speculate that starburst-dominated objects may indeed exist within the CHYT sample, since LSL observed only the most compact 31 objects out of the CHYT sample of 40 and the remaining 9 less compact objects may be the best candidates for being starburst-dominated. The lack of AGN-dominated objects may indicate that there is some sort of physical link between the starburst and the AGN in these dust-enshrouded objects; *eg.* the size of the starburst controls the fuel rate to the nucleus or the power of the AGN controls the size of the starburst it triggers.

An alternative explanation of the few 100 parsec scale radio emission is that it originates from synchrotron plasma well mixed with the dense molecular gas, as in the CHYT picture, but that star formation is not required to produce this plasma and that it ultimately originates instead from the obscured AGN. As discussed above in the context of possible origins for the RQ component in AGNs, the central AGN power source in a ULIRG could convert a characteristic proportion of its luminosity to mechanical energy, which drives particle-accelerating shocks into the surrounding dense interstellar medium. The resulting radio emission would be qualitatively indistinguishable from starburst-related emission using current data. While such a mechanism is clearly plausible, we must then explain why the free-free corrected radio flux densities from the ULIRGs conform to the standard FIR-to-radio correlation. This correlation is normally explained in terms of the link with massive stars. The number and size of these stars determine both the energy input for dust heating via photospheric UV radiation, and the supernova-driven energy input for synchrotron plasma via shocks. We instead speculate that the ratio of FIR-to-radio luminosity is determined by the fundamental properties of the dusty gas. We suggest that the input of radiative and mechanical energy to this material, by massive stars or a central AGN, leads to a characteristic radio/FIR spectral energy distribution that depends little on the details of the energy source.

If this picture is correct, it is possible that any starburst that is in progress in these objects may be energetically insignificant. The galaxies could then be viewed as youthful AGNs, normal in all respects except for the presence of a dense circumnuclear shroud

of dusty and molecular material. This shroud is heated and shocked by the AGN, and emits copious IR and radio emission in proportion characteristic of dusty gas clouds. This picture is compatible with our recent result that the OH megamaser in Arp 220 is located on pc scales, probably in a dusty molecular torus surrounding the AGN, and that most of the observed infrared power must have originated in or very near the torus to provide a sufficient reservoir to pump the maser (Lonsdale *et al.* 1991).

Although we have concluded from the analysis presented in this paper that it is quite possible for a dust-enshrouded RQQ to power the infrared emission from the ULIRGs, we have not, of course, proved that an RQQ *does* power the emission. If the question is approached from the opposite direction and one asks whether there is sufficient power in a nuclear starburst to power the observed far-infrared luminosity then a similar conclusion is reached: the observed nuclear radio continuum and H α luminosities appear to be consistent with a starburst interpretation of the far-infrared emission, after suitable extinction correction at H α , without requiring the presence of an additional AGN energy source (CHYT; Armus, Heckman and Miley 1989), but this does not prove that an AGN does not contribute to the emission.

The definitive observational test with which to try to discriminate between these possibilities would be to map the radio emission in detail on size scales intermediate between current VLBI data and the CHYT 8.4 GHz VLBA images. Initial attempts at phase-referenced imaging with the VLBA are currently underway. We can speculate that an AGN origin for the intermediate scale radio emission would lead to a more centrally condensed brightness distribution, corresponding to a central concentration of mechanical energy density, and perhaps to an asymmetric non-spherical geometry. In particular we might expect structure similar to that of Seyfert galaxies such as NGC 5518 (Wrobel 1990), which shows a bipolar appearance without high collimation.

We wish to thank Dave Sanders for discussions about the Sanders *et al.* (1989) comprehensive work on continuum distributions of BQS quasars which motivated our attempts to investigate bolometric luminosity correlations, Matt Malkan for providing us with H α spectra from Sun and Malkan (1989) and John Stocke for providing clarification on the work of SMWF. We thank an anonymous referee for

comments which have helped to clarify the discussion. HES and CJL **also** thank Haystack Observatory for hospitality while this work was being undertaken. The research described in this publication was carried out in part by the Jet Propulsion Laboratory, California Institute of Technology, under a contract with the National Aeronautics and Space Administration. Haystack Observatory is sponsored by the NSF under contract with the Northeast Radio Observatory Corporation.

REFERENCES

- Antonucci, R. R. J. and Barvainis, R. E. 1988, *Astrophys. J.*, **332**, L13.
- Armus, L., Heckman, T., and Miley, G. 1989, *Astrophys. J.*, **347**, 727.
- Barvainis, R. E. 1990, *Astrophys. J.*, 353, 419.
- Barvainis, R. 1993, *Astrophys. J.*, 412, 513.
- Burbidge, G. R., Jones, T. W. and O'Dell, S. L. 1972, *Astrophys. J.* 193, 43.
- Canizares, C. R. and White, J. L. 1989, *Astrophys. J.*, 339, 27.
- Condon, J. J., Huang, Z-P., Yin, Q. F., and Thuan, T. X. 1991, *Astrophys. J.* 378, 65 (CHIYT).
- Helou, G., Soifer, B. T., and Rowan-Robinson, M. 1985, *Astrophys. J. Lett.*, 298, L7.
- Isobe, T., Feigelson, E. D., and Nelson, T. I. 1986, *Astrophys. J.*, 306, 490.
- Kellermann, K., Sramek, R., Shaffer, D., Green, R., and Schmidt, M. 1989, *Astron. J.*, 98, 1495.
- Lonsdale, C. J. and Barvainis, R. 1994, *in preparation*.
- Lonsdale, C. J., Diamond, P. J., Smith, H. E., and Lonsdale, C. J. 1994, *Nature*, 370, in press.
- Lonsdale, C. J., Smith, H. E., and Lonsdale, C. J. 1993, *Astrophys. J. Lett.*, 405, L9 (L S1).
- Miller, L., Peacock, J. A. and Meade, A. R. G. 1990, *Mon. Not. R. Astr. Soc.* **244**, 207.
- Neugebauer, G., Green, R. F., Matthews, K., Schmidt, M., Soifer, B. T., and Bennet, J. 1987, *Astrophys. J. Suppl.* 63, 615.
- O'Brien, P. T., Gondhalekar, P. M., and Wilson R. 1988, *Mon. Not. R. Astr. Soc.*, **233**, 801.
- Puetter, R. C., Burbidge, E. M., Smith, H. E. and Stein, W. A. 1982, *Astrophys. J.*, 257, 487.
- Sanders, D. B., Phinney, E. S., Neugebauer, G., Soifer, B. T., and Mathews, K. 1989, *Astrophys. J.*, 327, 29.
- Schmidt, M. and Green, R. F. 1983, *Astrophys. J.*, 269, 352.
- Scoville, N. Z. 1992, in *Relationships between Active Galactic Nuclei and Starburst Galaxies*, ed. A. V. Filippenko (ASP:San Francisco), J), 159.
- Smith, H. E., Lonsdale, C. J., and Lonsdale, C. J. 1994, *in preparation*.
- Soifer, B. T., Boehmter, L., Neugebauer, G., and Sanders, D. 1989, *Astron. J.*, 98, 766.
- Stoike, J., Morris, J. L., Weymann, R. J., and Foltz, C. B. 1992, *Astrophys. J.*, 396, 487 (SMW1).
- Sun, W.-H. and Malkan, M. A. 1989, *Astrophys. J.*, 346, 68.
- Tannenbaum, H., Avni, Y., Green, R. F., Schmidt, M., and Zamorani, G. 1986, *Astrophys. J.*, 305, 57.
- Visnovsky, H. L., Impey, C. D., Foltz, C. B., Hewett, P. C., Weymann, R. J., and Morris, J. L. 1992, *Astrophys. J.*, 391, 560.
- Wilkes, B. J. and Elvis, M. 1987, *Astrophys. J.*, 323, 243.
- Wrobel, J. 1990, *Bull. Am. Astron. Soc.*, 22, 1316.

This 2-column preprint was prepared with the AAS L^AT_EX macros v3.0.

TABLE I
BQS SAMPLE

QSO	z	$\log \nu_{rest}$ optical data		$\log L_O$	$\log L_{O-UV}$	$\log \nu_{UV}$	$\log L_{O-X1}$	$\log L_{O-X2}$	$\log L_{IR-X2}$	$\log \nu_{IR}$	$\log P_{Total}$ (6cm)	$\log P_{Core}$ (6cm)
(1)	(2)	(3)	(4)	(5)	(6)	(7)	(8)	(9)	(10)	(11)	(12)	(13)
$\langle \log L_{int} \rangle$				11.67	12.09		12.54	12.74	12.98			
0003+15s	0.45	14.29	15.13	12.21	12.64	5.30	13.17	13.39	...		26.20	25.80
0007+106	0.09	13.51	15.01	11.06	11.50	5.30	12.11	12.28	12.38	12.74	24.71	24.38
0026+129	0.14	13.53	15.01	11.37	11.81	5.30	12.30	12.51			23.32	21.92
0043+039	0.38	14.27	15.11	11.84	12.16	5.50	12.32	12.41		...	22.91	<22.91
0044+030	0.62	14.34	5.18	12.22	12.61	5.30	13.00	13.18		...	25.58	25.32
0049+171	0.06	13.94	5.00	10.29	10.69	5.30	11.33	11.46		...	21.71	21.73
0052+251	0.15	13.53	5.01	11.37	11.82	5.30	12.34	12.53	12.61	2.76	22.56	22.45
0117+213	1.49	13.87	5.37	13.21	13.61	5.37	15.18	14.92		...	24.31	<24.31
01574001	0.16	13.54	5.01	11.27	11.72	5.30	12.15	12.44	12.82	2.54	23.65	23.49
0804+761	0.10	13.51	5.01	11.38	12.01	5.30	12.55	12.87	12.91	2.74	22.68	22.29
0838+770	0.13	13.53	5.01	10.81	11.43	5.30	11.86	12.16	12.28	2.53	<21.72	<21.72
0841+349	0.06	13.50	5.01	10.79	11.11	5.44	11.38	11.52	1.72	2.50	21.40	<21.31
0923+201	0.19	13.9s	5.01	11.37	11.91	15.30	12.36	12.69	22.28	<22.28
0946+301	1.22	14.47	5.25	12.94	13.33	15.72	13.63	13.69	<23.95	<23.95
0947+396	0.21	14.21	5.01	11.13	11.55	15.30	11.95	12.17	2.54	2.56	22.44	22.33
0953+414	0.24	14.00	5.06	11.77	12.19	15.42	12.67	12.87	23.37	<23.37
1001+051	0.16	14.19	5.00	11.08	11.52	15.30	11.96	12.19	2.31	2.76	22.63	<22.13
1004+130	0.24	13.57	5.06	11.83	12.12	15.43	12.34	12.46	2.68	2.79	25.74	24.52
1008+133	1.28	14.49	5.32	12.11	13.37	15.50	13.83	13.99	4.48	3.44	<23.45	<23.45
1011-010*	0.06	14.15	4.31	10.53	10.1s	15.30	11.30	11.68	1.84	2.72	21.27	21.39
1012+008	0.18	14.20	5.01	11.30	11.73	15.30	12.17	12.41	22.86	22.72
1018-090	0.34	14.26	5.10	11.81	12.29	15.30	12.81	13.01	26.26	25.15
1048+342	0.17	14.20	5.01	11.04	11.45	15.30	11.84	12.07	<22.04	<22.04
1049-005	0.36	14.26	5.10	11.85	12.29	15.30	12.75	12.99	3.24	2.83	23.14	<22.86
1100+772	0.31	14.03	5.09	11.86	12.28	15.30	12.81	12.99	3.05	2.82	26.16	25.22
1103-006	0.42	14.28	5.12	11.86	12.28	15.54	12.57	12.68	3.22	2.85	26.31	25.51
1114-415	0.14	13.97	5.01	11.03	11.36	15.44	11.49	11.55	2.10	12.76	21.97	21.93
1115+080	1.72	14.56	15.37	3.30	13.73	15.78	14.11	14.14	<24.31	<24.31
1115+407	0.15	14.19	15.01	0.92	11.32	15.30	11.73	11.96	22.17	<22.09
1116+215	0.18	13.9s	15.01	1.74	12.19	15.30	12.62	12.86	23.26	23.10
1119+120	0.05	13.49	14.99	0.42	10.80	15.30	11.23	11.45	1.64	12.50	21.65	<21.07
1121+422	0.23	14.22	15.06	1.21	11.55	15.30	11.93	12.14	<22.30	<22.30
1126-041	0.06	13.93	14.99	0.68	11.17	15.30	11.52	11.93	2.06	12.50	21.56	<21.25
1148+549	0.97	14.42	15.25	2.88	13.26	15.30	13.69	13.92	4.26	12.77	24.55	24.31
1151.1117	0.18	14.20	15.01	11.09	11.51	15.30	11.90	12.13			<22.11	<22.11
1202+281	0.17	13.54	15.01	10.12	11.32	15.43	11.91	11.97	12.23	12.54	22.67	22.56
1206+459	1.16	14.46	15.30	13.02	13.39	15.30	13.78	14.00	14.57	13.03	<24.14	<24.14
1211+143	0.081	13.51	15.01	11.35	11.75	15.42	12.27	12.41	12.50	12.51	22.06	<22.06
1216+069	0.33	14.25	15.01	11.96	12.26	15.30	12.59	12.73			24.00	24.00
1222+228	2.05	14.61	15.45	13.51	13.87	15.58	14.22	14.31		...	26.35	26.31
1226+023	0.16	13.54	15.01	12.32	12.76	15.30	13.30	13.47	13.57	12.54	27.28	26.52
1221+2011	0.06	13.50	15.00	10.71	11.23	15.30	11.79	2.08	12.14	12.73	21.73	21.38
1241+176	1.27	14.49	15.32	13.22	13.51	15.32	13.90	4.10			27.00	26.85
1244+026	0.05	14.15	14.99	10.14	10.39	15.37	10.83	0.88	11.25	12.72	21.57	21.33
1247+267	2.01	14.61	15.45	13.62	14.02	15.68	14.39	4.47			25.27	25.14
1248+401	1.03	14.44	15.26	12.71	13.08	15.30	13.46	3.68	14.36	13.01	<23.66	<23.66
1254+047	1.02	14.44	15.25	12.71	13.10	15.58	13.30	3.36			23.91	<23.91
1259+593	0.47	14.30	15.14	12.17	12.56	15.54	12.98	3.12			<23.11	<23.11
1302-102	0.29	14.24	15.08	12.12	12.64	15.30	13.13	3.42			26.15	26.15

TABLE 1— *Continued*

QSO	z	log ν_{rest} optical data		log L_O	log L_{O-UV}	log ν_{UV}	log L_{O-X1}	log L_{O-X2}	log L_{IR-X2}	log ν_{IR}	log P_{Total} (6cm)	log P_{Core} (6cm)
(1)	(2)	(3)	(4)	(5)	(6)	(7)	(8)	(9)	(10)	(11)	(12)	(13)
$< \log L_{int} >$				11.67	12.09		12.54	12.74	12.98			
1307+085	0.15	13.53	15.01	11.33	11.64	15.32	12.09	12.22	22.24	<22.24
1309+355	0.18	14.21	15.01	11.31	11.67	15.30	12.02	12.23	24.58	24.56
1310-108	0.01	14.14	14.9s	10.01	10.52	15.30	11.06	11.32	20.79	<20.77
1329+412	1.93	14.60	15.44	12.30	13.33	15.62	13.84	13.97	24.60	24.51
1333+176	0.55	14.32	15.16	12.14	12.52	15.30	12.91	13.13	25.28	25.36
1338+416	1.22	14.48	15.32	12.81	13.24	15.32	13.72	13.96	14.37	13.42	<23.99	<23.99
1351+236	0.06	14.15	14.99	10.281	10.56	15.30	10.79	10.96	11.71	12.50	21.49	<21.17
1351+640	0.09	13.51	15.01	11.12	11.50	15.30	11.75	12.08	12.29	12.51	23.30	23.48
1352+183	0.16	14.19	15.01	11.14	11.58	15.30	12.06	12.24	22.11	<22.11
1352+011	1.12	14.46	15.25	12.77	13.22	15.30	13.70	13.95	<23.78	<23.78
1354+213	0.30	14.24	15.0s	11.22	11.69	15.30	12.17	12.41	<22.53	<22.53
1402+261	0.16	14.19	15.01	11.29	11.76	15.30	12.20	12.46	12.63	12.54	22.54	<22.14
1404+226	0.10	14.17	15.11	10.60	10.98	15.30	11.29	11.55	22.29	22.23
1407+265	0.94	14.42	15.26	12.72	13.11	15.66	13.68	13.75	25.32	24.89
1411-1442	0.09	13.95	15.01	10.8s	11.26	15.30	11.66	11.88	12.09	12.74	21.98	21.92
1415+451	0.11	14.18	15.01	10.80	11.19	15.30	11.61	11.84	12.10	12.52	22.02	<21.82
1416-129	0.13	14.18	15.01	11.43	12.14	15.30	12.6N	13.02	23.09	22.43
1426+015	0.09	13.94	15.00	11.19	11.57	15.41	12.11	12.28	12.37	12.73	22.25	22.14
1427+480	0.22	14.22	15.06	11.09	11.50	15.30	11.87	12.09	<22.34	<22.34
1431-067	0.13	14.18	15.01	11.23	11.74	15.30	12.27	12.54	21.81	21.81
1440+356	0.08	13.94	15.00	10.86	11.27	15.30	11.71	11.95	12.13	12.51	22.29	21.93
1444+407	0.27	14.23	15.07	11.54	11.97	15.30	12.34	12.56	12.87	12.58	<22.71	<22.71
1448+273	0.07	13.91	15.00	10.75	11.07	15.30	11.40	11.60	11.74	12.73	21.93	21.93
1504+106	0.04	13.92	14.98	10.66	11.06	15.30	11.58	11.78	11.85	12.71	21.58	21.10
1512+370	0.37	13.61	15.11	11.81	12.15	15.50	12.53	12.6N	26.05	25.29
1519+226	0.14	13.96	15.01	10.95	11.44	15.30	11.81	12.19	22.76	<22.76
1522+101	1.32	13.84	15.31	13.16	13.63	15.31	14.15	14.10	24.24	<24.18
1534+580	0.03	13.92	14.98	10.01	10.46	15.30	10.97	11.22	11.33	12.49	21.53	21.50
1535+547	0.04	13.49	14.99	10.26	10.58	15.30	10.89	11.09	11.27	13.10	21.12	<21.12
1543+489	0.40	13.62	15.12	11.73	12.14	15.30	12.59	12.83	13.12	12.62	23.60	<23.60
1545+210	0.27	14.23	15.07	11.71	12.17	15.30	12.71	12.89	26.05	24.69
1552+085	0.12	13.96	15.01	10.92	11.16	15.30	11.29	11.40	11.75	13.45	22.36	<22.36
1612+261	0.13	13.53	15.01	10.99	11.45	15.30	12.02	12.23	23.25	22.76
1613+658	0.13	13.52	15.01	11.09	11.53	15.30	12.07	12.33	12.49	12.53	23.01	22.42
1617+175	0.11	13.52	15.01	11.18	11.86	15.30	12.38	12.76	22.46	<22.46
1626+554	0.13	14.18	15.01	10.90	11.40	15.30	11.90	12.16	21.79	22.06
1631+377	1.47	14.30	15.36	13.09	13.50	15.72	13.96	14.04	<24.05	<24.05
1634+706	1.33	13.84	15.32	13.72	14.13	15.32	14.53	14.81	14.90	12.84	25.13	24.88
1700+518	0.29	13.58	15.08	11.96	12.22	15.30	12.35	12.46	12.96	12.59	24.13	23.59
1704+608	0.37	13.61	15.11	11.97	12.33	15.30	12.66	12.85	13.06	12.84	26.59	24.40
1718+481	1.08	14.23	15.26	13.31	13.68	15.30	14.05	14.27	26.70	26.59
2112+059	0.47	13.64	15.14	12.42	12.92	15.30	13.49	13.75	13.80	12.86	23.62	23.46
2130+099	0.06	13.50	14.99	10.85	11.43	15.30	11.99	12.30	12.37	12.72	22.18	21.98
2201-1181	0.07	13.50	15.00	10.74	11.23	15.30	11.76	12.04	24.45	24.43
2233+134	0.33	13.59	15.09	11.60	12.11	15.30	12.58	12.87	23.06	22.84
2251+113	0.32	14.03	15.09	11.97	12.37	15.30	12.67	12.99	26.09	23.67
2302+029	1.04	14.22	15.25	12.97	13.53	15.30	14.09	14.35	24.08	23.83
2314+092	0.68	13.70	15.17	12.49	12.96	15.30	13.42	13.63	13.71	12.92	27.31	27.31

Table 2
Statistical Results

	Cox-Hazard		BHK		EMM Regression Fit					
	χ^2 (1° freedom)	P_{score}	Kendall's τ	P_{score}	$a \pm \sigma_a$	$b \pm \sigma_b$	σ_{fit}	$a \pm \sigma_a$	$b \pm \sigma_b$	σ_{fit}
(1)	P_{total} (2)	P_{score} (3)	P_{total} (4)	P_{score} (5)	(6)	P_{total} (7)	(8)	(9)	P_{score} (10)	1
BQS	97/16	97/40	97/16	97/40		97/16			97/40	
l_0	64.4	41.1	0.98	0.74	1.23 ± 0.15	9.09 ± 1.75	1.31	1.33 ± 0.17	7.31 ± 1.98	1.40
l_0-IV	62.7	40.3	0.97	0.74	1.21 ± 0.15	8.75 ± 1.83	1.32	1.32 ± 0.17	6.85 ± 2.02	1.41
l_0-X1	61.3	38.0	0.95	0.73	1.13 ± 0.15	9.17 ± 1.87	1.35	1.26 ± 0.17	7.06 ± 2.14	1.45
l_0-X2	58.1	37.3	0.92	0.70	1.16 ± 0.15	8.66 ± 1.95	1.36	1.28 ± 0.18	6.44 ± 2.25	1.46
BQS*	61/8	61/29	61/8	61/29		61/8			61/29	
l_0	49.5	26.3	1.09	0.64	1.26 ± 0.12	8.40 ± 1.38	0.50	1.29 ± 0.18	7.68 ± 2.00	0.66
l_0-IV	47.0	25.4	1.07	0.63	1.18 ± 0.13	8.69 ± 1.46	0.53	1.21 ± 0.19	7.99 ± 2.15	0.70
l_0-X1	45.1	25.1	1.05	0.61	1.09 ± 0.13	9.26 ± 1.56	0.56	1.14 ± 0.19	8.26 ± 2.33	0.75
l_0-X2	38.9	22.1	1.00	0.59	1.02 ± 0.13	9.86 ± 1.62	0.59	1.07 ± 0.20	8.86 ± 2.40	0.78
UIP/BIG		92/43		92/43					92/43	
l_0		4.9		0.35				0.77 ± 0.20	13.7 ± 2.30	0.93
l_0-IV		13.8		0.50				1.12 ± 0.20	8.85 ± 2.32	0.82
l_0-X1		26.1		0.53				1.13 ± 0.18	8.39 ± 2.12	0.78
l_0-X2		25.7		0.50				0.99 ± 0.17	9.96 ± 2.00	0.80

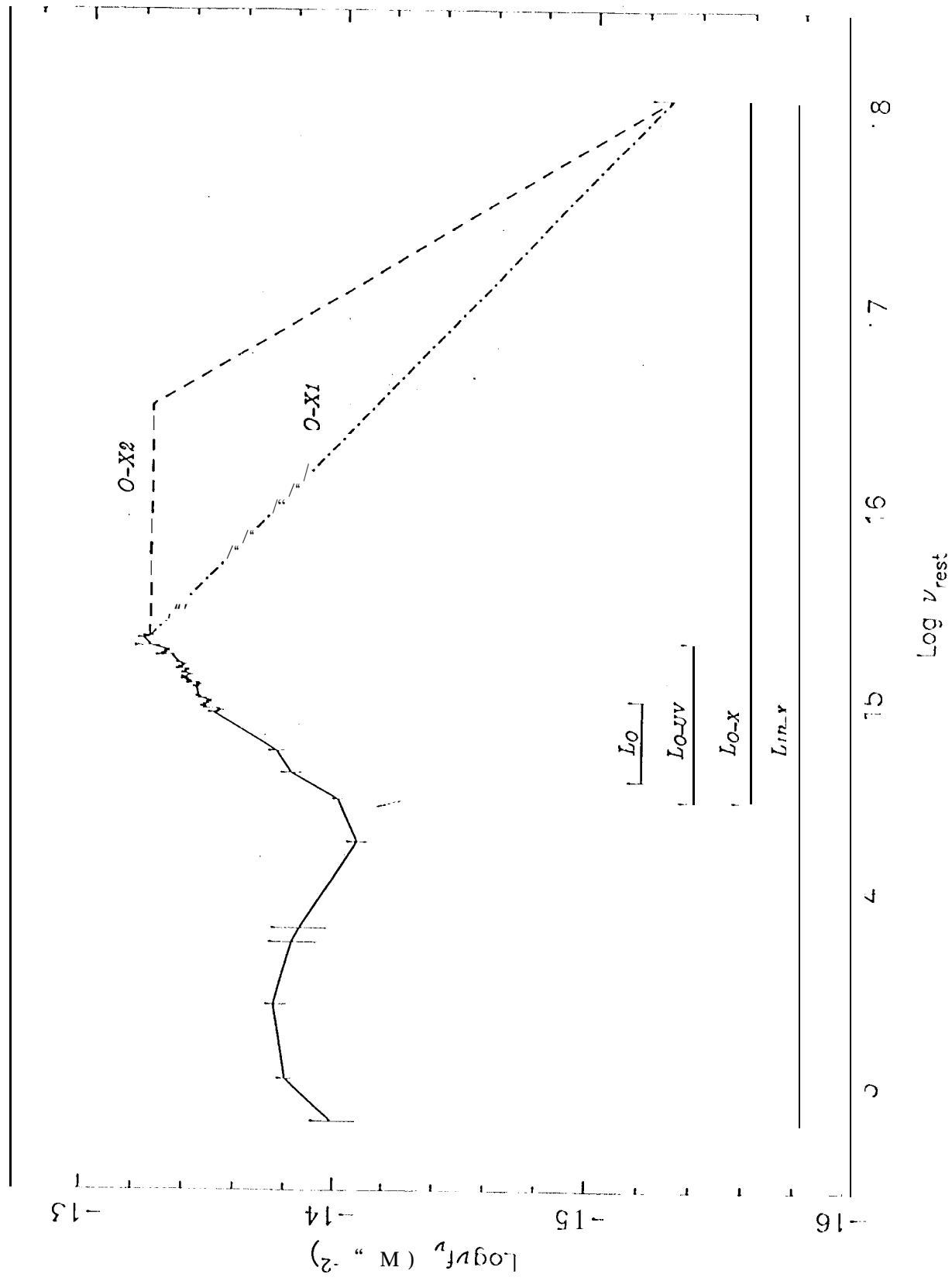
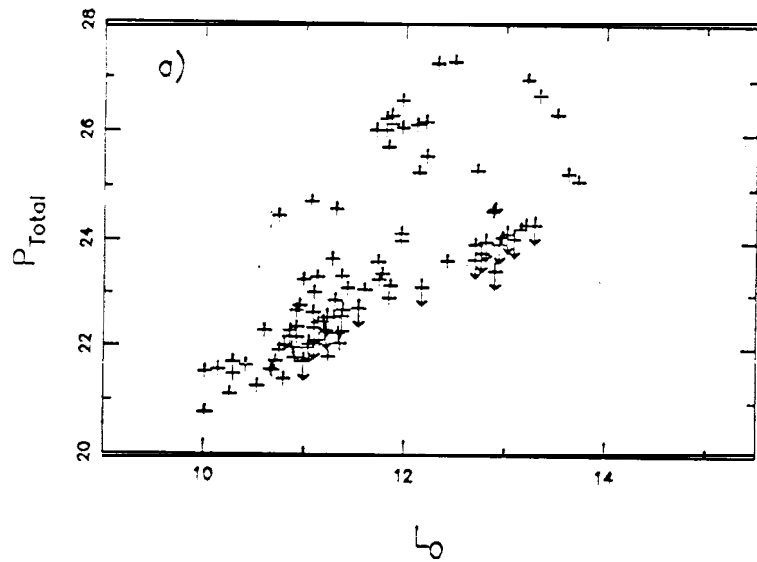
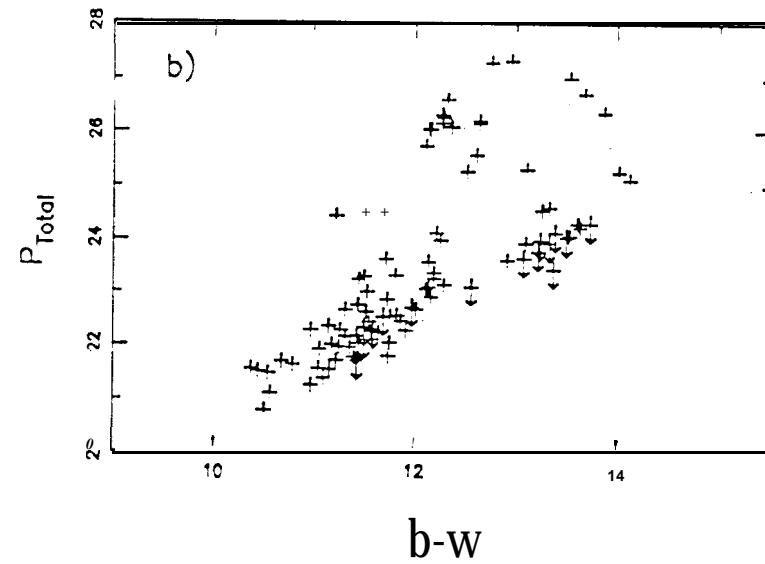


Figure 1: Schematic illustration of the integrated luminosities calculated in this paper. The spectrum of the BQS QSO PG1634+706 has been plotted from the infrared to the X-ray region. The intervals for the integrated luminosities O , $O-UV$, $O-X1$ & $O-X2$, and $IR-X1$ & $IR-X2$ are marked. The dash-dot line indicates the interpolation for L_{0-X1} and the dashed line indicates the interpolation for L_{0-X2} .

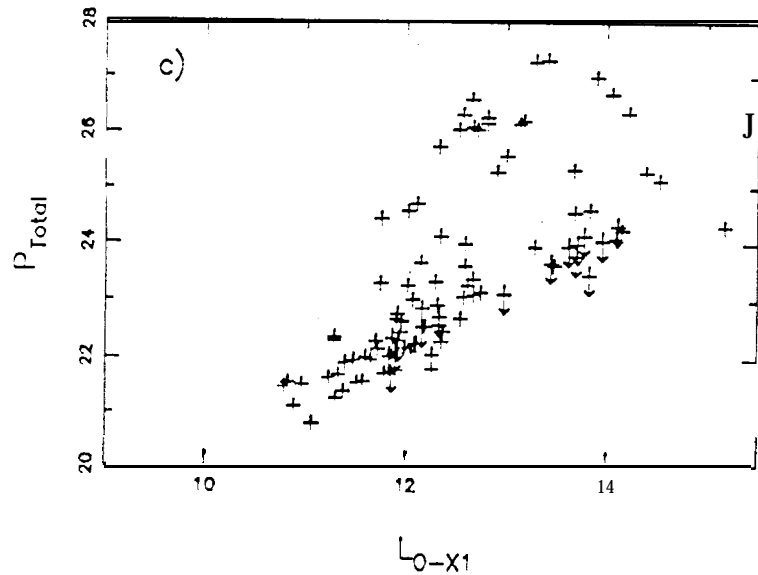
BQS - 6 cm Radio Tots' Power 'vs. Integrated Luminosity (O)



BQS - 6 cm Radio Total Power vs. Integrated Luminosity (O-UV)



BQS - 6 cm Radio Total Power vs. integrated Luminosity (O-X?)



BQS - 6 cm Radio Total Power vs. Integrated Luminosity (O-X2)

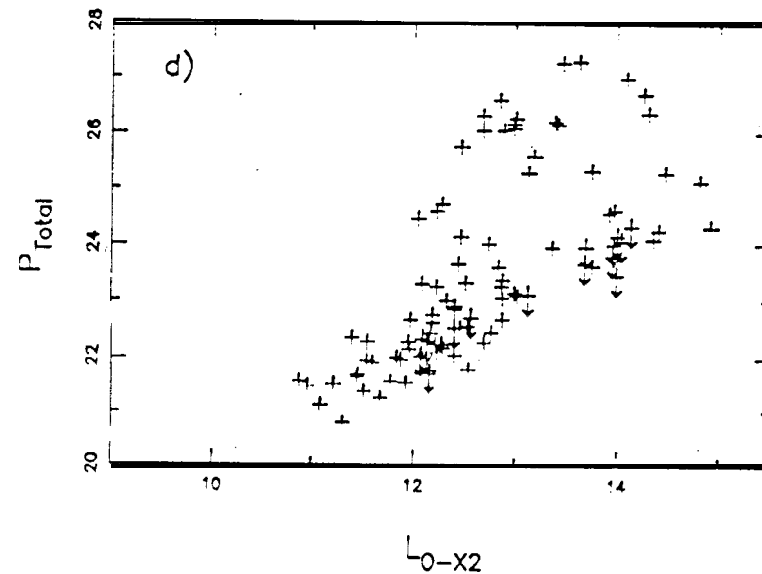
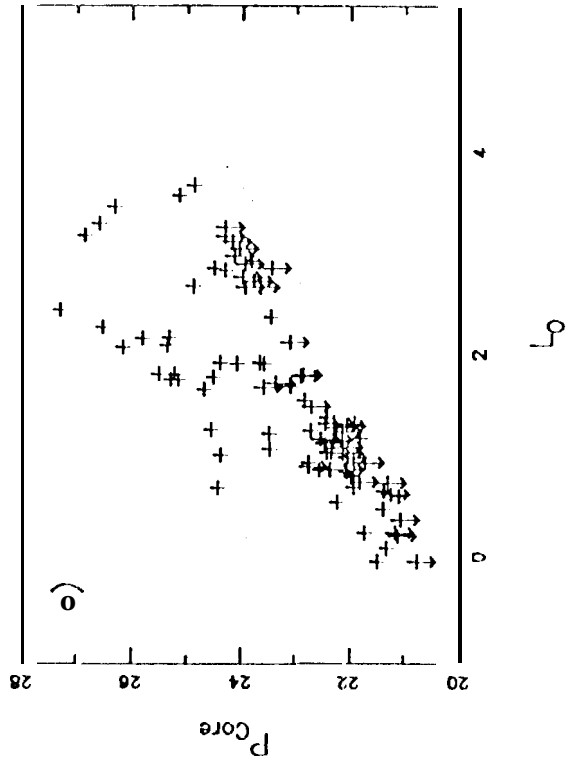
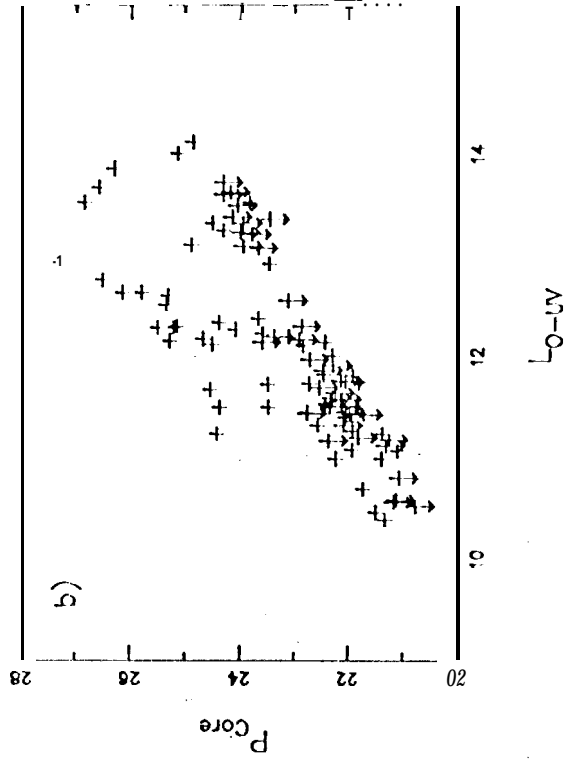


Figure 2: The Total 6cm Radio Power vs Integrated Luminosity for the 97 BQS quasars in our sample. a) P_{Total} vs. Optical Luminosity ($\log \nu_{rest} = 14.6 - 15.0$) as defined in the text. b) P_{Total} vs. Optical-UV Luminosity ($\log \nu_{rest} = 14.5 \rightarrow 15.3$). c) P_{Total} vs. Optical-X-ray Luminosity ($\log \nu_{rest} = 14.6 - 17.8$) calculated by method #1. d) P_{Total} vs. Optical-X-ray Luminosity calculated by method #2.

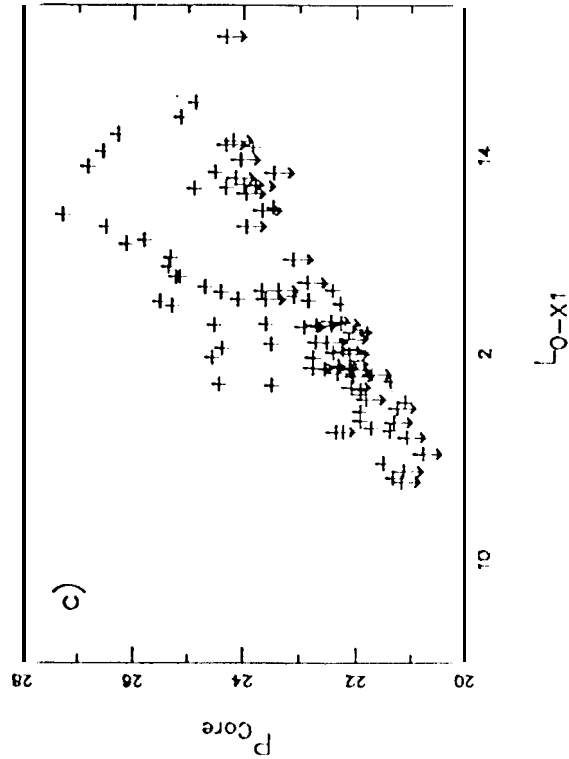
BQS - 6 cm Radio Core Power vs. Integrated Luminosity (O)



BQS - 6 cm Radio Core Power vs. Integrated Luminosity (O-UV)



BQS - 6 cm Radio Core Power vs. Integrated Luminosity (O-X1)



BQS - 6 cm Radio Core Power vs. Integrated Luminosity (O-X2)

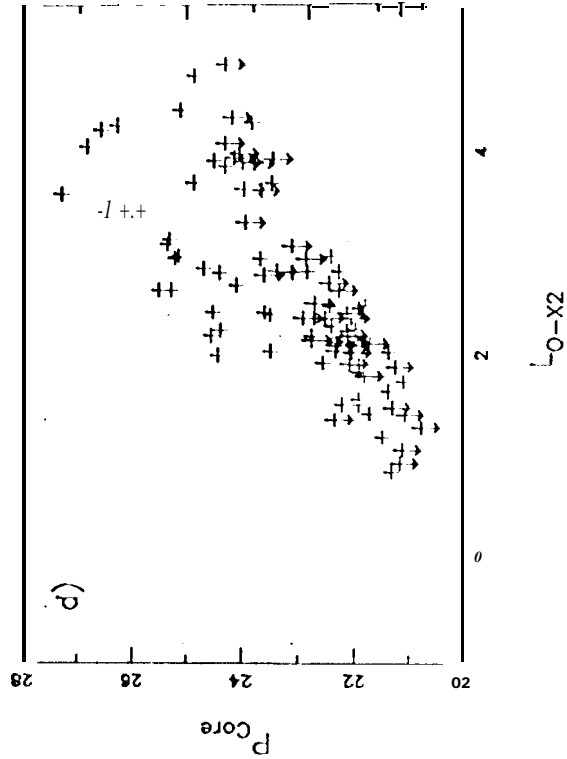


Figure 3: The 6cm Radio Core Power vs Integrated Luminosity for the 97 BQS quasars in our sample. a) P_{Total} vs. Optical Luminosity ($\log \nu_{\text{rest}} = 14.6 \rightarrow 15.0$) as defined in the text. b) P_{Total} vs. Optical-UV Luminosity ($\log \nu_{\text{rest}} = 14.5 \rightarrow 15.3$). c) P_{Total} vs. Optical-X-ray Luminosity ($\log \nu_{\text{rest}} = 14.6 \rightarrow 17.8$) calculated by method #1. d) P_{Total} vs. Optical-X-ray Luminosity calculated by method #2.

BQS ($Z < 0.6$; $\log R < 1.0$) – 6cm Radio Core Power vs. integrated Luminosity (O-X2)

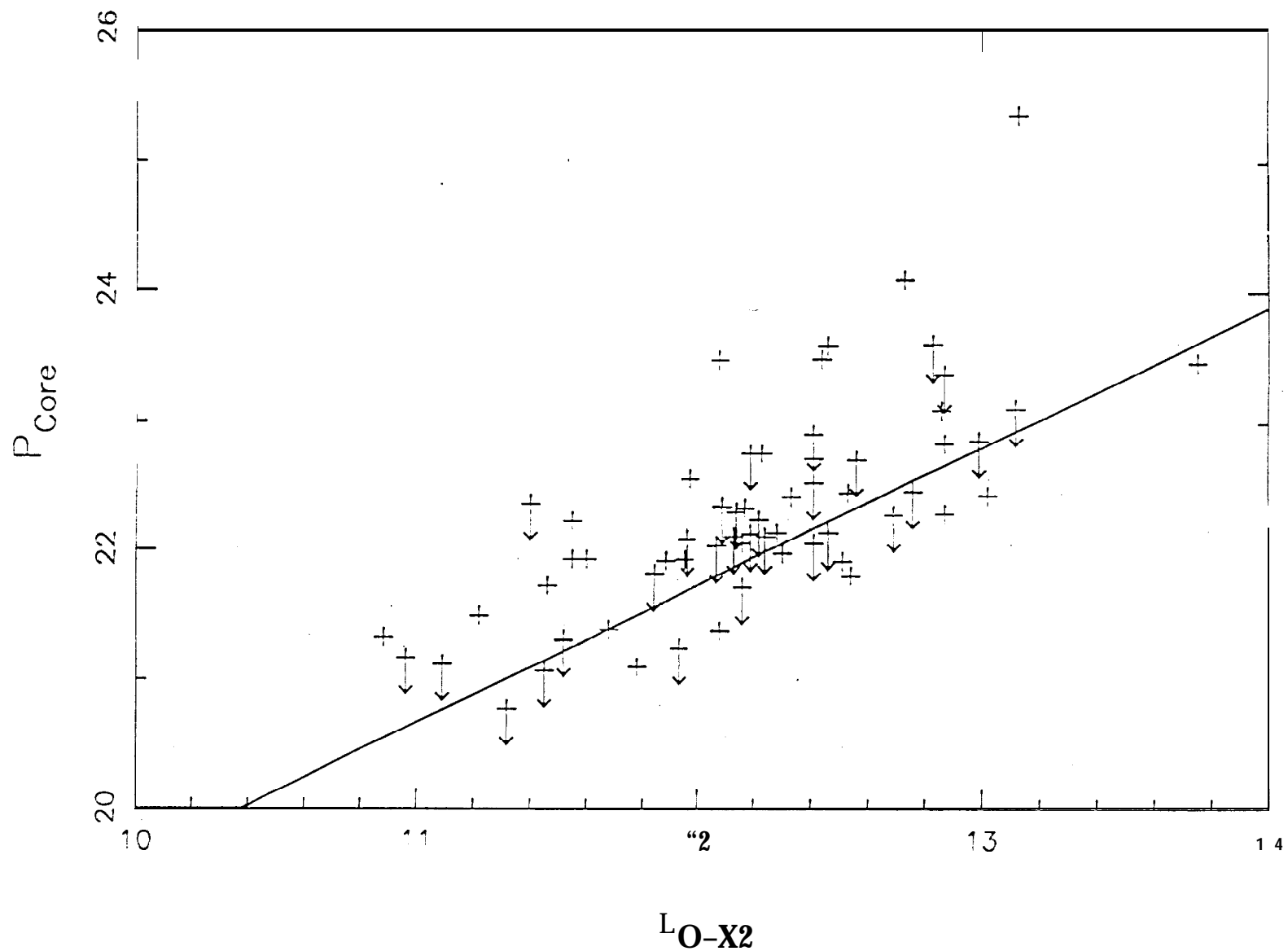


Figure 4: The 6cm Radio Core Power vs Integrated Optical-X-ray Luminosity for a subsample of the BQS ($z < 0.6$; $\log R < 1.0$). The straight line is a regression fit by EM Method: $\log P_{\text{Core}} = 1.07 \cdot \log L_{\text{O-X2}} - 1.885$.

BQS ($z < 0.6$; $\log R < 1.0$) and VLB Sample — 6 cm Core Power vs. $L(\text{Bol})$

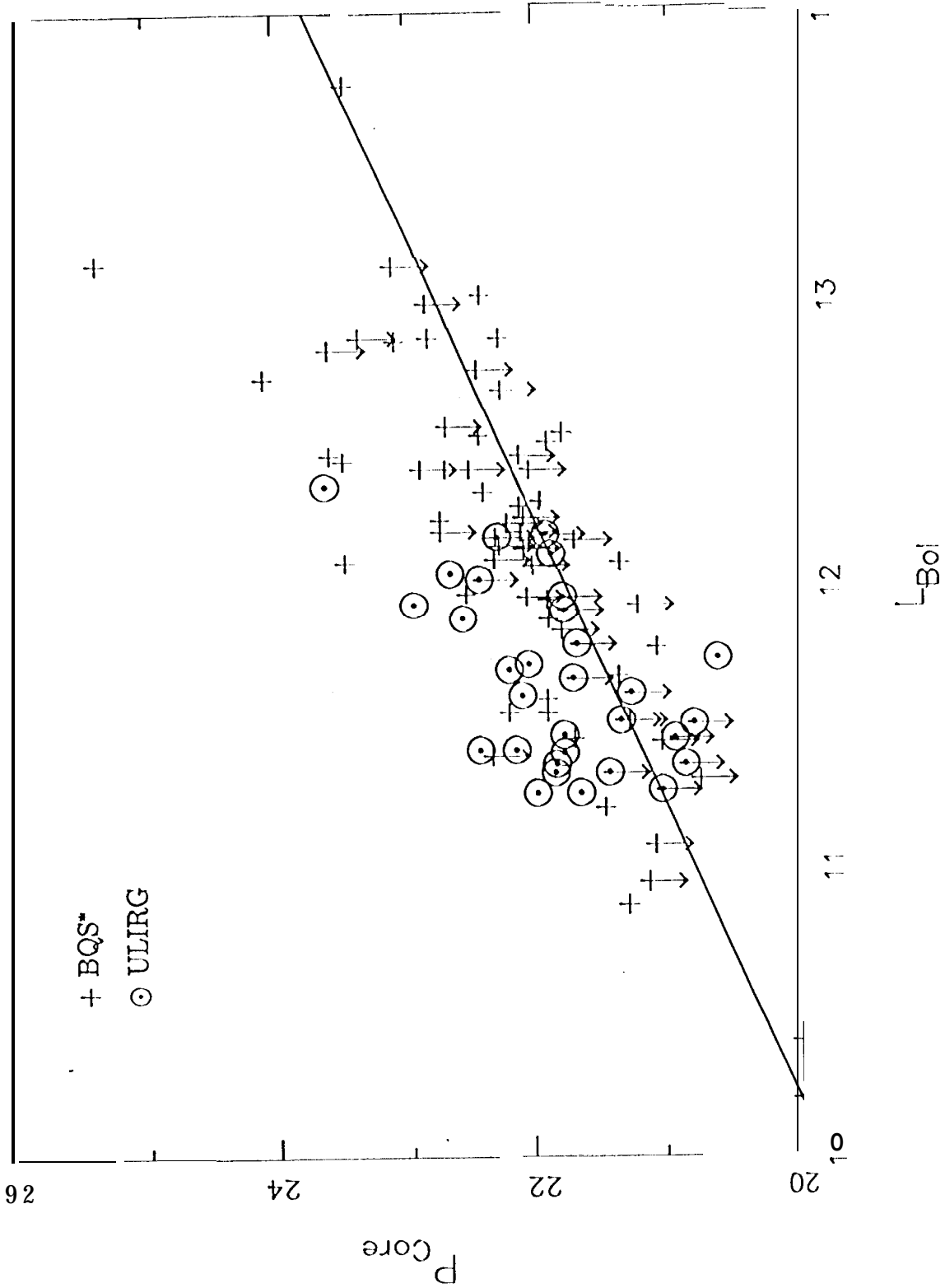


Figure 5: The 6cm Radio Core Power vs Bolometric Luminosity for the combined BQS* subsample ($z < 0.6$; $\log R < 1.0$) plus our sample of 31 Ultraluminous Infrared Galaxies. The straight line is a regression fit by EM Method: $\log P_{\text{Core}} = 0.99 \cdot \log L_{\text{Bol}} + 9.96$. For the BQS* sample, the Bolometric Luminosity is taken to be $L_{\text{O-X2}}$ as in Figure 4; for the ULIRGs L_{Bol} is taken to be L_{IR} as described in the text.